Adv Polym Sci (2013) 252: 29–64
DOI: 10.1007/12_2012_174

Published online: 7 August 2012

Probing Properties of Polymers in Thin Films Via Dewetting

Günter Reiter

Abstract In our quest to make functional devices smaller, the thickness of polymer films has reached values even smaller than the diameter of the unperturbed molecule. Many experimental studies have been devoted to the determination of the behavior of such thin films as a function of film thickness and temperature. However, despite enormous efforts over the last few decades, our understanding of the origin of some puzzling properties of such thin films is still not satisfactory and several peculiar observations remain rather mysterious. In this context, we explore the consequences of film preparation, i.e., the transition from a dilute polymer solution to the glassy state, with respect to the properties of polymers in thin films. This transition is likely to result in residual stresses arising from out-of-equilibrium chain conformations due to rapid solvent loss. Consequently, depending on thermal history and ageing time, such films exhibit significant changes even in the glassy state, which we can quantify by performing detailed studies of visco-elastic dewetting of thin polystyrene films on solid substrates. We explore relaxation times, residual stresses, and temporal changes to the stability of non-equilibrated thin films as they progress toward stable equilibrium behaviors. We present some tentative ideas on the relation between the observed atypical mechanical and relaxational behavior and the metastable states introduced by sample preparation.

Keywords Aging · Dewetting · Film preparation · Glass transition · Relaxation times · Residual stress · Thin polymer films

G. Reiter (✉)
Physikalisches Institut, Fakultät für Physik und Mathematik, Albert-Ludwigs-Universität Freiburg, Hermann-Herder-Strasse 3, 79104 Freiburg, Germany
e-mail: guenter.reiter@physik.uni-freiburg.de

Contents

1 Introduction and Historical Remarks on Thin Polymer Films

A large number of studies on thin polymer films revealed that various physical properties exhibited characteristics strongly deviating from their bulk behavior, with major implications for most technological applications based on such nanoscopic films. Diverse measurements have shown anomalous irreversible and reversible density changes after annealing below the bulk glass transition temperature (T_g) [1–9], unexpected instabilities of these films [1, 10–13], unusual ageing [14–21], deviations in mobility [22–28], deformed chain conformations [29–32], dewetting processes independent of molecular weight and much faster than suggested by bulk visco-elasticity [17–49], clear indications for residual stresses within these spin-coated thin polymer films [17, 39–54], a thickness-dependent but also history-dependent T_g [55–85], and fast relaxation processes [17, 43, 48, 52–54]. A lowered softening temperature and decreased interfacial diffusion (employing the same samples) are examples of seemingly contradictory polymer dynamics in thin films. The cause of these deviations is a matter of ongoing debate [86–97].

Despite an extensive number of publications, it is becoming increasingly obvious that a clear understanding of thin polymer film properties has not yet been reached [87, 88, 91, 94–97]. The origin of (some of) these puzzling properties of thin polymer films is still not satisfactorily understood. At present, we are still missing a consistent understanding of the influence of film preparation and confinement on chain conformations. It is not yet clear how the visco-elastic behavior of thin polymer films is affected by the resulting chain conformations, in particular on approaching T_g. It is disputable whether or not the transition from a mostly dilute solution to a dry glassy state introduces a "conformational state" with its "own" properties [4, 94].

In the typical case of film preparation from solution, the solvent evaporates rapidly (within seconds) with a concomitant increase in polymer concentration until the film solidifies while there is still a significant amount of solvent present in the film. It is not certain whether the initially highly separated molecules in solution have enough time to interpenetrate sufficiently in order to establish an equilibrium state of entangled polymers. It is plausible that films prepared this way contain molecules having frozen-in conformations far from equilibrium, with a reduced

degree of inter-chain overlap [43, 48]. Thus, one may ask if film preparation and the resulting non-equilibrium conformations of the polymers have an influence on measurements of visco-elastic properties, film stability, T_g, diffusion coefficient, etc. Sample preparation might also represent a possible cause for the anomalous behavior in glassy thin polymer films. In particular, fast evaporation of the solvent during the widely used process of spin-coating [98–101] could potentially produce samples that are far from equilibrium.

In trying to answer these questions it is certainly instructive to examine previous fundamental experimental works in which such thin films have been employed. In particular, we have to mention studies on polymer interdiffusion in which thin polymer films were used for testing theoretical concepts of polymer physics [102–106]. Spin-coating was typically used to prepare the films because this process presents an easy way of obtaining smooth film of precisely controllable thickness, even in the nanometer range. This is an essential criterion for investigating, for example, polymer diffusion across an interface between two films. While these experiments successfully supported the model of chain reptation [102–106], they also indicated some deviations that hinted, for example, at the enrichment of chain ends at surfaces [104, 106].

The possibility of being able to change easily and controllably the film thickness by varying the concentration of the solution used for spin-coating opened up a whole field of research on questions related to the chain-like nature of these macromolecules. In particular, at that time it was unclear (and partially still is!) if polymer properties like viscosity, chain conformation (as expressed for example by the radius of gyration), chain orientation, and interdiffusion rate, or mechanical properties and T_g change once the thickness of the film decreases below the diameter of Gaussian polymer coils in bulk samples [1].

Unexpectedly, several of these experiments turned out to be “failures” in the sense that the films were not stable and were “destroyed” in the course of annealing above the glass transition temperature of the bulk system ($T_{g,bulk}$), and even below $T_{g,bulk}$ the films were unstable [1]. Stability, however, was required in order to allow for chain diffusion. Thin polymer films were often characterized by reflectometry techniques [1, 3, 102–106]. In the context of unstable films, reflectometry indicated a severe “roughening” of the films during annealing [1]. Consequently, it was necessary to investigate the origin of instabilities and to identify the relevant parameters in order to obtain stable films that do not roughen in time.

Two simple aspects helped to gain some insight into the origin of the roughening process. First, use of polished silicon wafers of high reflectance allowed detection of the homogeneity of the films by detecting the uniformity of the interference color. Second, inspection of thin films by optical microscopy made it clear that the instability of the film was related to a retraction of the film from the substrate, i.e., the film dewetted the substrate [107]. While it was soon found that dewetting could easily be avoided by using different substrates or by applying various cleaning procedures for the substrates, the dewetting phenomenon itself attracted significant attention [107–120]. It turned out that polymers are convenient fluids for dewetting studies because their negligible vapor pressure (polymers are nonvolatile) ensured

mass conservation and their typically rather high viscosity assured that the dewetting process was slow enough to allow simple, time-resolved measurements. Moreover, the possibility of tuning the film thickness in the nanometer range enabled testing of the influence of short- and long-range intermolecular forces on film stability and dewetting dynamics [121–131]. In addition, as the process is highly sensitive to changes in interfacial properties and the properties of the dewetting fluid, dewetting can also be considered as a kind of rheological tool for the investigation of thin film properties [42, 43, 46].

The phenomenon of dewetting, i.e., the retraction of a fluid from a surface it was forced to cover, is frequently observed in our everyday life and is of central importance in many technological applications as well as in a variety of physical and biological systems [108, 132]. The wettability of a surface by a liquid is to a large extent characterized by interfacial tensions and thus by the contact angle. However, it is difficult to investigate kinetic effects like friction (energy dissipation) at an interface by contact angle measurements alone. The necessary velocity-dependent information is provided by spreading or dewetting experiments. Dewetting experiments are attractive because of their simplicity, sensitivity, and rapidity. Dewetting allows linking of static and kinetic molecular and interfacial properties (and variants of these properties) with macroscopically observable parameters like dewetting velocity and shape of the rim.

Despite its simplicity with respect to experimental observation, dewetting turned out to be extremely sensitive to even tiniest changes in the system under investigation. Thus, dewetting has proven to be a highly successful and time-efficient tool for obtaining time-resolved information on a molecular scale, allowing determination of interfacial properties and their changes in real time and in situ. Thus, dewetting experiments can provide information about relaxation and ageing processes of polymers in the film.

2 Dewetting: Theoretical Considerations

In general, if a substrate has a lower surface tension than a fluid, this fluid will not form a stable film when deposited onto such a substrate. Consequently, such an unstable fluid film will retract from this substrate by a dewetting process [108–111]. This process is the result of driving forces that try to remove the fluid and of dissipative processes that reflect the resistance of the fluid to its removal.

Here, we try to provide a elementary view on dewetting that nonetheless covers all essential features relevant in the context of thin polymer films. Thus, we neglect gravity (because the mass of the film is extremely small) and inertia (because we investigate cases where the dewetting velocity is comparatively small). We first concentrate on the simple case of a Newtonian fluid on a smooth and solid substrate. Accordingly, we assume that the fluid is completely characterized by its viscosity, i.e., we initially exclude visco-elastic, shear thinning or thickening, and temporal effects. Moreover, we assume that the substrate is inert and does not generate hysteretic behavior, i.e., we exclude contact line pinning and chemical reactions at the substrate.

The displacement of the three-phase contact line, where the fluid film meets the substrate and the surrounding medium (in most cases this is air), is governed by the balance of driving and resisting forces. For a Newtonian fluid, capillarity represents the main driving force for dewetting. It is related to an imbalance between the three interfacial tensions [γ_L (liquid–air), γ_{LS} (liquid–substrate), and γ_S (substrate–air)] that meet at the contact line and are responsible for a dynamic contact angle θ_{dyn}. In contrast, when all interfacial tensions are balanced we obtain the equilibrium contact angle θ_{equ} (which represents the absolute minimum in free energy of the system) and the contact line will be at rest [133]. Dewetting is thus driven by a capillary force (uncompensated Young force, F_{Young}) that arises from the difference between θ_{dyn} and θ_{equ}. In fact, on ideal surfaces, whenever the contact angle deviates from θ_{equ} the contact line will show the tendency to move in order to try to (re-)establish equilibrium. In general, the stronger θ_{dyn} deviates from θ_{equ}, the faster will be the movement of the contact line. Thus, for $\theta_{dyn} \neq \theta_{equ}$, a net force F_{Young} (per unit length of the contact line) pushes the contact line:

$$F_{Young} = -\gamma_S + \gamma_{LS} + \gamma_L \cdot \cos\,\theta_{dyn}. \tag{1}$$

Using the relation for the equilibrium contact angle, $\gamma_S = \gamma_{LS} + \gamma_L \cdot \cos\,\theta_{equ}$, we obtain $F_{Young} = \gamma_L(\cos\,\theta_{dyn} - \cos\,\theta_{equ})$.

For small contact angles, the cos term can be approximated by the first term of its series expansion, i.e., $\cos\,\theta \approx 1 - (1/2)\theta^2$. This then leads to:

$$F_{Young} = (1/2) \cdot \gamma_L(\theta_{equ}^2 - \theta_{dyn}^2). \tag{2}$$

Removing the fluid from the substrate involves the relative movement of molecules past each other. This gives rise to viscous dissipation within the fluid. The motion of fluid molecules at the substrate causes frictional losses. Furthermore, depending on fluid–substrate interactions and properties of substrate and fluid, these frictional losses may be localized in a region close to the contact line (no slip boundary condition). For strong cohesion of the fluid, as is the case for entangled polymers, one may encounter slippage of the fluid on top of the substrate and thus frictional losses originate from the whole region moving (slipping) past the substrate. As a general feature, it is important to note that interfacial friction is responsible for the formation of a rim, i.e., the accumulation of the removed fluid in a region close to the contact line. Without such friction or in cases where interfacial friction is small compared to viscous dissipation within the fluid, the removed fluid will be distributed within the remaining surrounding film, causing an increase in mean film thickness but no formation of a rim.

The no-slip condition at the substrate reflects the fact that liquid molecules at a solid substrate experience (significant) interactions responsible for adhesion. In contrast to liquid molecules in contact with other liquid molecules, they do not move easily on this substrate. As a consequence, the velocity of these molecules is approximately zero (hence, no-slip boundary condition). However, applying this boundary condition strictly would not allow for any displacement of a liquid on a

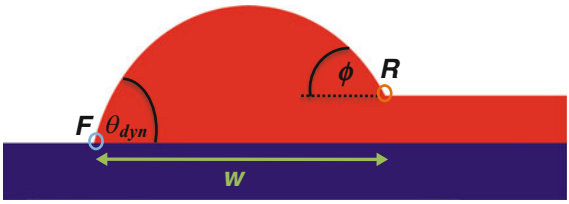

Fig. 1 Rim formation in the course of dewetting of a thin liquid film. At the front position F of the rim, the contact angle assumes its dynamic value θ_{dyn} and at the rear position R it takes the value ϕ. The width of the rim is given by w

solid substrate. Thus, to account for the experimental fact that contact lines can and do move, various approximations, partially based on molecular mechanisms, have been proposed (see e.g. [134]). In general, a cut-off length, typically as small as the size of the molecules, has to be introduced [132, 135].

For small contact angles, the flow pattern close to the contact line (the wedge region) can be approximated by the so-called lubrication approximation, which compares the flow in the wedge with flow in a thin film. The velocity of fluid molecules is only determined by their distance vertical to the substrate; the molecules move preferentially in the direction parallel to the substrate and less in the direction away from the substrate.

If the viscous forces are significantly smaller than the surface tension (as expressed by a capillary number Ca much less than 1: $Ca = U{\cdot}\eta/\gamma_L$, with U being the velocity of the contact line and η the viscosity of the liquid), the shape of a liquid drop can be reasonably well approximated by a spherical cap. Laplace pressure P_{L} (where $P_{\mathrm{L}} = 2{\cdot}\gamma_{\mathrm{L}}{\cdot}K$ and the curvature $K = 1/R$ for a spherical cap of radius R and thus $P_{\mathrm{L}} = 2{\cdot}\gamma_{\mathrm{L}}/R$) will be able to assure the same curvature everywhere (with the possible exception of the region very close to the contact line, where long-range molecular interactions, e.g., van der Waals forces, may become important).

The liquid removed from the dried region (e.g., a hole in the fluid film) is collected in a ridge (the "rim") (see Fig. 1). The shape of this rim may be described approximately as a portion of a cylinder that is characterized by two contact angles θ_{dyn} and ϕ (see Fig. 1).

In the case of a no-slip boundary condition, the movement of the contact line (position F) with dewetting velocity U results from a balance between driving force and viscous dissipation in the wedge close to the moving contact line. Integration over the whole moving part of the fluid from its lowest thickness at the contact line having a minimum thickness of h_{min} to its thickest part with the maximum thickness of h_{max} yields the total viscous force F_{visc} per unit length of the contact line during dewetting [132, 134]:

$$F_{\mathrm{visc}} = 3\eta/\theta_{\mathrm{dyn}} \cdot U \cdot \ln(h_{\mathrm{max}}/h_{\mathrm{min}}), \tag{3}$$

$$F_{\mathrm{Young}} = (1/2) \cdot \gamma_{\mathrm{L}}(\theta_{\mathrm{dyn}}^2 - \theta_{\mathrm{equ}}^2) = 3\eta/\theta_{\mathrm{dyn}} \cdot U \cdot \ln(h_{\mathrm{max}}/h_{\mathrm{min}}) = F_{\mathrm{visc}}. \tag{4}$$

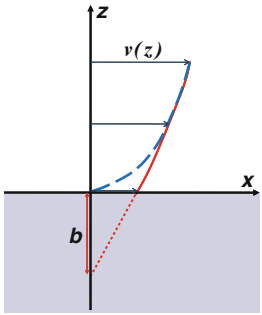

Fig. 2 Velocity profile of liquid flow within a thin film (lubrication approximation). For the no-slip boundary condition (*dashed line*), the velocity at the substrate ($z = 0$) is zero. In the case of slippage (*solid line*), the liquid velocity is not zero at the substrate surface and only extrapolates to zero at a distance b (slippage length) within the substrate

For dewetted distances much larger than the width of the rim, both ends of the rim (denoted by F and R in Fig. 1) move at approximately the same velocity. Moreover, at the position R the equilibrium value of the contact angle is zero (rim in contact with the film of the same liquid) and thus yields:

$$(1/2) \cdot \gamma_{\mathrm{L}} \cdot \theta_{\mathrm{dyn}}^2 = 3\eta/\theta_{\mathrm{dyn}} \cdot U \cdot \ln(h_{\mathrm{max}}/h_{\mathrm{min}}). \tag{5}$$

Here, h_{max} and h_{min} are evaluated at the position R.

Assuming that the Laplace pressure is the same everywhere within the rim (i.e., the same curvature is assumed to exist everywhere in the rim) requires that $\theta_{\mathrm{dyn}} \approx \phi$. For thin films in the nanometer range and a size of the rim in the range of micrometers, the logarithmic factors at positions R and F are similar. Consequently, a highly useful relation is obtained between dynamic and equilibrium contact angles for the case of viscous dewetting (with $\theta_{\mathrm{dyn}} \approx \phi$): [136]:

$$\gamma_{\mathrm{L}}(\theta_{\mathrm{dyn}}^2 - \theta_{\mathrm{equ}}^2) \cdot \theta_{\mathrm{dyn}} = \gamma_{\mathrm{L}}\phi^3, \tag{6}$$

$$\theta_{\mathrm{dyn}} = \theta_{\mathrm{equ}}/\sqrt{2}. \tag{7}$$

This yields a constant dewetting velocity U of:

$$U \sim \gamma_{\mathrm{L}}/\eta \cdot \theta_{\mathrm{equ}}^3 \sim U^* \cdot \theta_{\mathrm{equ}}^3. \tag{8}$$

Basically the same procedure can be applied to the case where the liquid is slipping on the substrate by introducing an extrapolation length (slippage length) b within the substrate (see Fig. 2) where the flow velocity would be zero, i.e., the non-slip boundary would be reached at a virtual interface inside the solid. Thus, one expects $h_{\mathrm{min}} \approx b$ [132]. Slippage is particularly relevant in the case of entangled

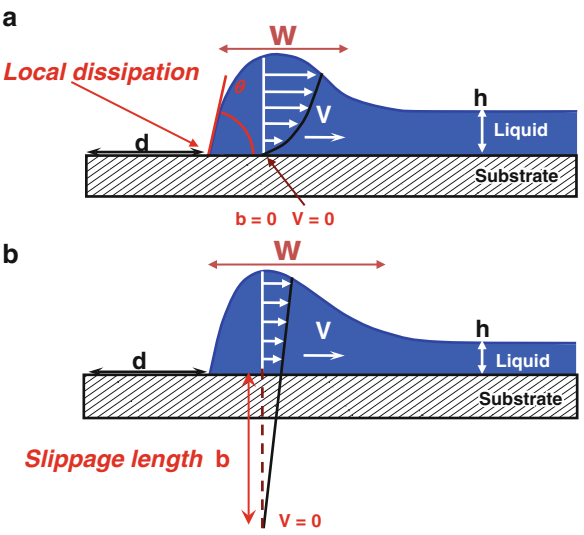

Fig. 3 Late stages of dewetting of a Newtonian fluid on a substrate with (**a**) non-slip and (**b**) slip boundary conditions; V velocity, W width of rim, h film thickness, d dewetted distance

polymer melts spreading or dewetting on a smooth surface [137–153]. A large number of experimental studies on slippage have been recently reviewed [154, 155].

In the case of slippage, the frictional dissipation F_{diss} (force per unit surface) at the interface between the liquid on the substrate is characterized by a friction coefficient ζ, and is proportional to the velocity V_{slip} with which the whole rim of width w is moving past the substrate: $F_{\mathrm{diss}} = \zeta \cdot V_{\mathrm{slip}}$. As has been shown by de Gennes, ζ is given by the ratio of fluid viscosity over slippage length, i.e., $\zeta = \eta/b$ [42, 46, 108]. The theoretical prediction for the length b in the steady-state flow of a polymer melt is $a \cdot (N^3/N_{\mathrm{e}}^2)$, where a is the monomer size, N is the polymerization index, and N_{e} the number of segments between entanglements [132, 137]. For a slippage length b larger than the film thickness h_0, the velocity of the dewetting fluid does not vary significantly in the direction normal to the substrate. Thus, the fluid roughly flows like a plug. In such a case, energy is dissipated almost exclusively at the liquid–substrate interface where the highest velocity gradient exists. Schematic views on the differences of the no-slip or slip boundary condition in the context of dewetting are given in Fig. 3. Thus, the frictional loss within the rim (force per unit length of the contact line) is:

$$F_{\mathrm{int}} \sim \zeta \cdot V_{\mathrm{slip}} \cdot w \sim \eta/b \cdot V_{\mathrm{slip}} \cdot w. \tag{9}$$

Consequently, for the opening of a hole of radius r in a film of thickness h_0, force balance $[(1/2) \cdot \gamma_{\mathrm{L}} \cdot \theta_{\mathrm{dyn}}^2 = \eta/b \cdot V_{\mathrm{slip}} \cdot w]$ and mass conservation $(r^2 h_0 \sim 2rw^2\theta_{\mathrm{dyn}})$ lead to ($V_{\mathrm{slip}} = \mathrm{d}r/\mathrm{d}t$):

$$\mathrm{d}r/\mathrm{d}t \cdot (r \cdot h_0)^{1/2} \sim (\gamma_{\mathrm{L}}/\eta) \cdot b \cdot \theta_{\mathrm{dyn}}^2 \tag{9a}$$

or

$$r^{3/2} \sim (\gamma_L/\eta)\theta_{dyn}^2(b/h_0^{1/2})t \tag{9b}$$

and thus the dewetting velocity decreases in time $V_{slip} \sim t^{-1/3}$.

Seminal work has been performed by Brochard-Wyart and colleagues [110–113, 144, 145] on dewetting of thin polymer films with thicknesses smaller than the slip length b (high-slip regime). Assuming a Newtonian fluid, they have determined a characteristic length $\Delta_0 = (h_0 \cdot b)^{1/2} = (h_0 \cdot \eta/\zeta)^{1/2}$, which is related to the transition between an initially viscous dissipation-dominated regime due to fluid flow in a flat film (the amount of fluid in motion is small and fluid motion at the interface concerns only a small distance less than Δ_0 away from the contact line) and a subsequent regime where dissipation due to friction at the film–substrate interface controls the dewetting velocity [42, 46, 145]. Consequently, one obtains three stages of hole opening [110–113, 144, 145].

For small holes ($R < \Delta_0$), viscous dissipation within the film due to radial and ortho-radial deformations dominate. This leads to an exponential growth of the hole, a consequence of a continuously increasing length of the three-phase contact line, i.e., the perimeter of the hole. During this regime, no rim is formed. For $R > \Delta_0$ interfacial friction dominates. At this later stage, the relative increase in hole perimeter is small and so the increase in driving force is smaller than the increase in frictional force. Thus, a rim of width Δ_0 starts to build up.

For dewetting from a straight edge (edge geometry), no initial exponential growth regime exists because the length of the three phase contact line always stays constant. Therefore, right from the onset of dewetting a rim of width Δ_0 builds up, accompanied by an initially constant dewetting velocity V. Once the rim is fully developed ("mature") at $R \sim b$, the dewetting velocity starts to decrease ($V \sim t^{-1/3}$) because now the width of the rim (and thus interfacial friction) increases with time [42, 46, 145].

During the regime of building up of a rim, the driving capillary force at the contact line, expressed by the spreading parameter $|S|$, is balanced by the viscous normal stress σ integrated over the total height H of the film at the front of the rim moving a dewetted distance $d(t)$:

$$|S| = -\sigma d(t) H \tag{10}$$

Rim build-up occurs at times t shorter than the relaxation time of the fluid in the film: $t < \tau = h_0 \cdot \eta/|S|$ [42, 46, 145].

Far away from the dewetting region, the fluid velocity decays to zero. At short times [i.e., at the onset of dewetting and rim build-up, when $h(x,t)$ is still close to h_0] these equations yield the velocity profile within the film as [42, 46]:

$$v(x,t) = V_0 \exp[-(x-d)/\sqrt{2\Delta_0}]. \tag{11}$$

It should be noted that a constant dewetting velocity for Newtonian liquids can only be observed as long as the assumption of a non-slip boundary conditions is satisfied, i.e., most dissipation takes place in the liquid wedge close to the contact line. Consequently, dissipation is independent of the actual size of the rim and will not change in the course of dewetting. However, in the case of slippage, a significant velocity gradient exists at the film substrate interface over the whole width of the rim. In this case, interfacial friction occurs over the whole moving interface, which is proportional to the width of the moving rim. Accordingly, as the size of the rim increases in course of dewetting, dissipation increases also. The driving capillary force, however, is constant and, consequently, the dewetting velocity decreases with time.

We will present a few examples, which demonstrate that the balance of forces enables us to extract in a highly quantitative manner detailed information on molecular and interfacial properties of thin polymer films from relatively simple dewetting experiments.

3 Dewetting Experiments Using a Newtonian Fluid

As dewetting reflects the balance of driving forces and energy dissipation, and thus is the consequence of intrinsic properties controlled by molecular interactions, this kinetic process is at all stages self-adjusting to any variations in experimental conditions, in particular at the solid–fluid interface. Thus, in following the displacement of a contact line in time we are able to determine velocity-dependent (kinetic) molecular interfacial properties at a polymer–polymer interface, such as friction (energy dissipation). As an example to demonstrate the capacity of such experiments, we use these kinetic aspects of dewetting in real time to investigate the properties of a polymer melt slipping on a layer of chemically identical molecules, end-grafted to a silicon substrate (i.e., a polymer brush). The entropy difference between grafted and free polymers results in autophobic behavior of the brush [146, 147, 156–161].

We are interested in the following questions: How does a polymer move or flow on its own monolayer, or more generally, how do macromolecules slide past each other? What are the consequences of the autophobic behavior between grafted and free polymers for dewetting? What is the value of the friction coefficient at such polymer–polymer interfaces? After a brief description of our experimental conditions, we present the experimental results, which are discussed in light of the theory described above. Finally, we show what we can learn about molecular parameters controlling interfacial properties.

Polydimethylsiloxane (PDMS) films represent a well-investigated example of dewetting of a Newtonian fluid. Here, we present experimental results on the dewetting behavior of thin films on smooth non-wettable silicon substrates that were coated with a layer of end-grafted PDMS molecules (a polymer brush) [146–149], because at high grafting densities an autophobic behavior was generated [146, 147], i.e., the free molecules dewetted the grafted layer.

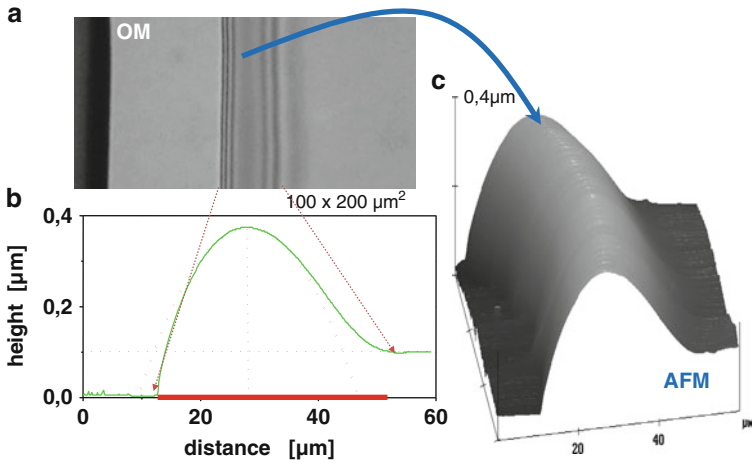

Fig. 4 (**a**) Optical micrograph (top view) of dewetting. (**b**) Cross-section and (**c**) 3D view of the shape of the rim as measured by AFM

The thickness h_0 of the PDMS films on top of the PDMS brush, as measured by ellipsometry, was varied in the range of 30–150 nm. All films were obtained by spin-coating dilute heptane solutions directly onto the coated substrates. As indicated in Fig. 4, isothermal dewetting of the thin polymer films, i.e., the retraction of a contact line, was followed in real time (t) by optical microscopy. The morphology of the rim was also investigated by atomic force microscopy (AFM). More details on sample preparation and dewetting measurements can be found in [146, 147].

An example of systematic analysis of an autophobic dewetting experiment is given in Fig. 5. It should be emphasized that it is possible to simultaneously measure the dewetted distance (d) and the width (w) of the rim by tracking the front (F) and rear (R) positions of the dewetting rim in time. As can be seen in Fig. 5, both d and w did not increase linearly in time, i.e., the dewetting velocity decreased in the course of dewetting. Fitting the data points for $d(t)$ to a power-law gave an exponent of 0.65 ± 0.05, which is consistent with the theoretically expected [112, 139] value of 2/3 for slippage of the liquid on the substrate [see Eq. (9) and the related transformations]. A constant dewetting velocity, on the other hand, would have indicated a non-slipping behavior. The slowing down of the dewetting process with time is thus a distinct feature that indicates slippage.

In addition to this temporal evolution of the dewetting velocity, slippage also invokes a characteristic dependence on film thickness. In the non-slip case, the dewetting velocity is independent of film thickness, but the rim width, for a given dewetted distance, is larger for thicker films. Thus, interfacial friction increases with film thickness and dewetting proceeds more slowly in thicker film. This is shown in Fig. 6.

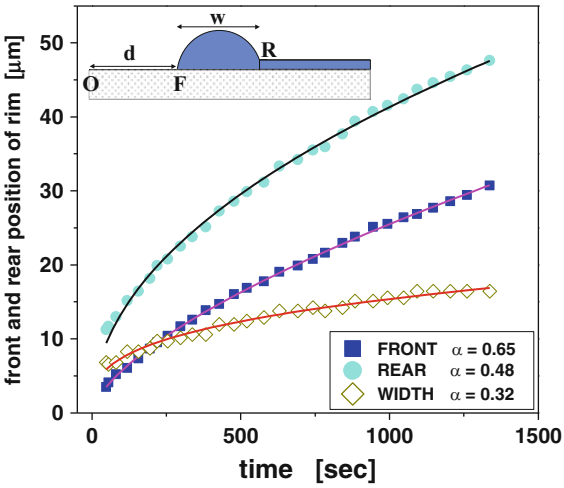

Fig. 5 Typical result for dewetting of a PDMS film (92 nm, $M_w = 308$ kg/mol) on top of a densely grafted brush of end-functionalized PDMS molecules (6.3 nm, $M_w = 8.8$ kg/mol). The temperature was 50°C. Dewetted distance d and the width w of the rim are represented in the *inset*. The *lines* are best fits of $y = A(t - t_o)^{\alpha}$ to the data, where y stands for d or w. A is a constant prefactor, and t_0 is a time offset. α was found to be 0.65 for d and 0.32 for w [146, 147]

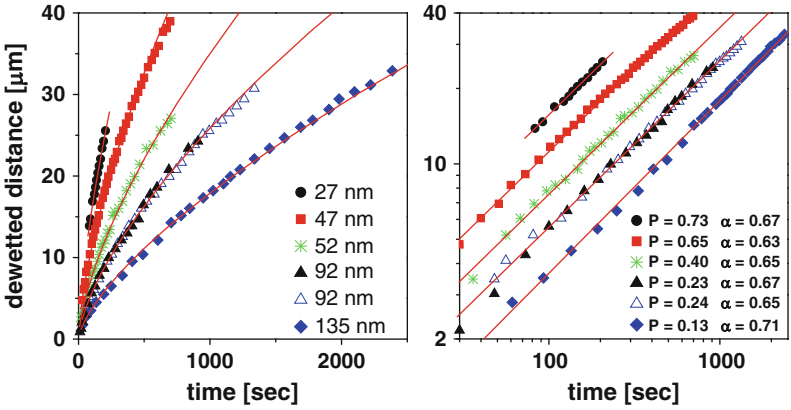

Fig. 6 Typical result for dewetting of a PDMS film [$M_w = 308$ kg/mol, $\eta(25°C) = 1{,}000$ Pa s] on top of a densely grafted layer of end-functionalized PDMS molecules (6.3 nm, $M_w = 8.8$ kg/mol) for different thicknesses, as indicated. *Left*: linear scale clearly shows the decrease in dewetting velocity with film thickness. *Right*: logarithmic scale demonstrates that all samples follow the same power law. The *solid lines* are best fits to the data using the equation $d \sim P(t - t_o)^{\alpha}$. As indicated, we obtained $\alpha = 0.65 \pm 0.05$ for all measurements at low temperatures (here, 50°C). The prefactors P, which depend on parameters like contact angle and slippage length, decreased with film thickness. Note that two independent measurements using the same sample gave the same results (*solid* and *open triangles*). Note further that films of similar thickness (47 and 52 nm) showed rather different prefactors P

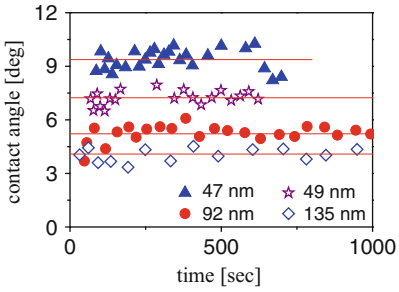

Fig. 7 Examples showing the temporal evolution of contact angle in the course of dewetting, as derived from mass conservation for the system described in Fig. 6 (for the film thicknesses indicated)

Based on mass conservation, measuring d and w for nonvolatile liquids like polymers as a function of time t allows determination of the value of the contact angle θ and even tracking of it in time and determination of possible variations of θ in time, without any fitting. For slipping films we get:

$$\theta(t) = d(t)h(t)/C \cdot w^2(t) \tag{12}$$

The constant C, accounting for the shape of the rim, has been found [112] to be 0.1 for slipping films. Typical results for autophobic dewetting of PDMS films are shown in Fig. 7. The values of θ differed between samples but were found to be constant in time, confirming the stability and homogeneity of the investigated dewetting system in the course of the experiments.

Similarly, we also can obtain the value of the slippage length b and its temporal evolution:

$$b(t_i) = 3\eta \cdot V(t_i)w(t_i)/(\gamma_L \theta^2(t_i)). \tag{13}$$

Note that this approach for measuring the contact angle and slippage length (see Fig. 8) also allows detection of changes in the adsorbed or grafted PDMS layer during the experiment (see [147]).

Interestingly, these results indicate that for the slow dewetting velocities of these experiments, b neither depended on dewetting velocity nor on film thickness. According to theory [see [112] and Eq. (9)], the viscous force F_V increases with w. Taking into account the balance of forces ($F_D = F_V$) and knowing that in the course of the dewetting experiments described in Figs. 5 and 6 the driving force characterized by θ (see Fig. 7) is constant, we anticipate that the dewetting velocity V decreases with the increase in w. This is indeed confirmed in Fig. 9, which proves that dissipation increases linearly with w. Such a relation between V and w implies that the whole rim slips.

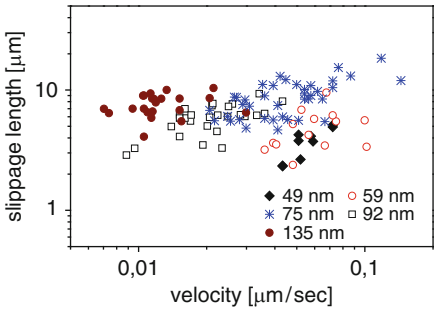

Fig. 8 Slippage length as determined from Eq. (13) as a function of dewetting velocity on double-logarithmic scales

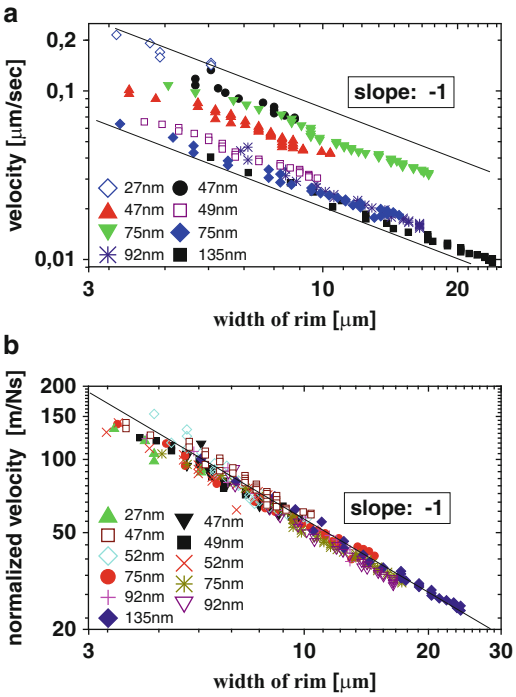

Fig. 9 (**a**) Dewetting velocity and (**b**) normalized velocity [multiplied by $b/(\gamma_L \cdot \theta^2)$] as a function of the width of the rim for various film thicknesses, as indicated

Moreover, when normalizing the velocity by the capillary driving force (proportional to θ^2) and the slippage length b (giving a parameter in units of meter per Newton second) allowed us to obtain a master curve (Fig. 9b) as expected from Eq. (9). We note that both θ and b were found to be constant in time

(see Figs. 7 and 8). We did not observe any systematic dependence of θ and b on film thickness h_0. This corroborates that the theoretical description of our observations takes all relevant parameters into account.

Besides viscosity η, the slippage length b mainly reflects the interfacial friction coefficient ζ (per area of one monomer): $b = \eta/\zeta$ [137]. Thus, for the observed values of $b \sim 10$ μm and the viscosity of the dewetting PDMS film ($\eta = 1{,}000$ Pa s we can deduce a value of $\zeta \sim 10^8$ Pa s/m. Comparing this value to the monomeric friction coefficient [141] $\zeta_0 = 3.7 \times 10^7$ Pa s/m indicates that only a few monomers at the interface contributed to friction ($\zeta \sim 3\zeta_0$). This implies that the free polymers penetrated only little into the layer of densely grafted, chemically identical polymers. In conclusion, this example shows that dewetting experiments are capable of relating friction at the brush–melt interface to the degree of interpenetration between grafted and free polymer chains.

4 Dewetting Experiments Using a Visco-Elastic Fluid: Polystyrene Films Slightly Above the Glass Transition Temperature

It is important to realize that in systems where a film is forced onto a substrate that it does not want to wet, the capillary force acts independently of the state of the liquid. Thus, even if the liquid is vitrified, a force is pushing the glassy film. Dewetting, however, may be stopped, at least on experimentally accessible time scales, because this acting force may be too weak to push a vitreous solid or a highly visco-elastic material. We will present some results, again obtained by using optical microscopy or AFM, showing how the dewetting process is affected by the visco-elastic properties of the film. In other words, we want to show what kind of information dewetting studies can provide about the rheological properties of thin polymer films.

It is well known that capillary forces resulting from intermolecular interactions are capable of retracting a purely liquid film from a solid surface [110]. It is, however, less frequent that one encounters a similar dewetting phenomenon for highly visco-elastic films where, on the time scale of the experiment, the material cannot flow like a liquid. Experiments on thin polystyrene (PS) films at temperatures not too far above T_g fall into this category. [107, 114–120] Under such conditions, the polymer can by no means be treated as a Newtonian liquid. Thus, interpretation of dewetting results has to also account for the highly elastic properties of the polymer film. However, it is not clear a priori if capillary forces alone, which are of the order of 10 mN/m, are strong enough to provoke dewetting in highly elastic films.

The elasticity of the film also affects characteristic features of dewetting like the shape of the rim or the temporal evolution of the hole diameter. In addition, in the course of time, the behavior of the PS film will switch from highly elastic at short

Fig. 10 Sample geometry indicating a PS film (glass transition around 105°C) on an adsorbed or grafted liquid-like PDMS layer supported by a silicon substrate

times to purely viscous at long times, which also becomes evident in the dewetting parameters and their temporal evolution. Thus, in order to shed some light onto the phenomenon of dewetting of highly elastic films, we followed the process of hole growth in PS films in detail, starting from the very early stages. To accentuate the possible influence of driving forces, and to reduce simultaneously the resistance resulting from interfacial friction, we chose highly non-wettable substrates, as achieved by using PDMS-coated Si wafers (Fig. 10). This PDMS coating "screened" all heterogeneities of the solid substrates and thus represented an ideally homogeneous surface of low surface energy and low interfacial friction for the moving PS film.

First, we investigated dewetting of PS films thinner than 20 nm using AFM at room temperature after annealing the samples ex situ in a closed hot stage purged with nitrogen. Only for thicker films, where holes became visible under an optical microscope, were real time investigations performed in situ.

In analogy to previous results [107, 114–120], all PS films on such substrates turned out to be metastable and ruptured upon annealing at elevated temperatures. The number density of holes increased rapidly with decreasing film thickness [107]. We concentrated on the shape of these holes and its evolution with time at temperatures above about 103°C. Complementary experiments indicated, however, that hole formation was also possible at lower temperatures [162]. As discussed previously [4, 17], hole formation may also reflect the relaxation of internal tensions induced during sample preparation and caused by confining the polymers to films thinner than the size of the unperturbed coil.

Figure 11 presents typical AFM results for the early stages of hole formation obtained from the thinnest films investigated. Due to the many holes of similar size formed within the small area detected by AFM, these films allowed us to conclude that most holes were formed within a narrow time interval at the very beginning. At such early stages, the material displaced from the dewetted areas was not collected in visible rims around these areas but was distributed evenly within the whole film in between the holes. Thus, imposing mass conservation, the film thickness between the holes had to increase. A comparison between the thicknesses before annealing as measured by ellipsometry and the depth of the holes measured by AFM is shown in Fig. 12.

For these two films from PS of very different molecular weights (125 kg/mol and 3,900 kg/mol) we found approximately the same dewetting behavior. This demonstrates that at these early stages the viscosity of the polymer, which varied

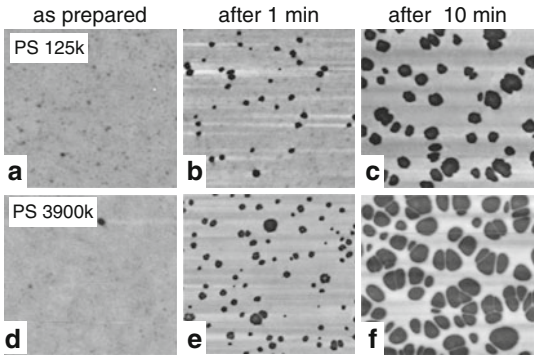

Fig. 11 Typical atomic force micrographs showing the consequences of annealing thin PS films on PDMS-coated Si wafers at a temperature close to the glass transition of PS. Rimless holes of some 100 nm in diameter are formed. Two different molecular weights are compared. *First row*: 16 nm PS with M_w of 125 kg/mol, *second row*: 13 nm PS with M_w of 3,900 kg/mol. (**a**, **d**) show the as-prepared samples. (**b**, **e**) and (**c**, **f**) were measured after annealing for 1 and 10 min at 105°C, respectively. The size of the images is 3 μm × 3 μm

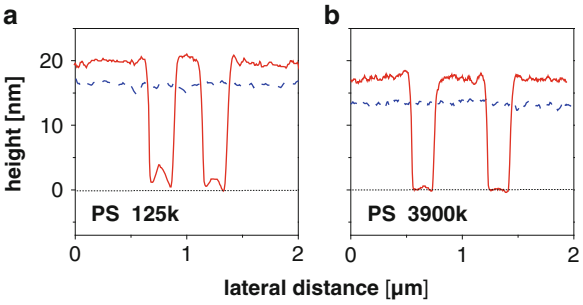

Fig. 12 (**a**, **b**) Cross-sections of the PS films shown in Fig. 11: *dashed line* as-prepared, *solid line* after annealing for 10 min at 105°C

by several orders of magnitude, did not play a determining role in the rate of hole growth. This result seems to indicate that the plateau shear modulus of PS, which does not depend significantly on chain length, may be the essential control parameter for the growth rate.

Figure 13 shows a quantitative comparison of our results for the early stages for hole growth. Almost all tiny holes (with a diameter D of about 70 nm) were formed after annealing for only 1 min. This implies an average opening velocity (dD/dt) of these holes of about 70 nm/min and an average shear rate $d\gamma/dt = 1/D \cdot dD/dt$ of about 0.7 min^{-1}. Comparing $d\gamma/dt$ with the reptation time (τ_{rep}) of PS close to T_g (for the conditions of the experiments shown in Fig. 11, τ_{rep} is much larger than one year [104]) demonstrates that on the time scale of the experiments we cannot expect

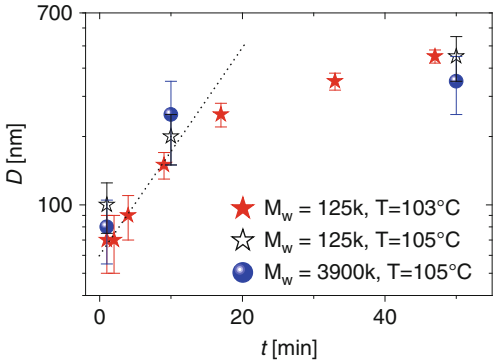

Fig. 13 Hole diameter D as a function of annealing time t for PS films of Fig. 11 annealed at 103°C and 105°C. Note that the molecular weight does not seem to have an influence on the growth rate. The *dotted line* represents an exponential fit to the early stages, yielding D (nm) = **67** (nm) exp[t/12.6 (min)]

viscous flow of the polymer. This makes it clear that the capillary driving force cannot be balanced by viscous dissipation only. Other resisting forces have to be invoked. Potential candidates are elastic or plastic deformation of the quasi-solid PS film and friction at the PS–PDMS interface.

As the annealing time increased, D became progressively larger. The data shown in Fig. 13 allowed the growth of the hole diameter at the earliest stages to be fitted to an exponential function, similar to the theoretical expectation [144], for the onset of hole growth when no rim is formed. However, the many holes per unit area started to coalesce as their diameters became larger than about 200 nm, which had an influence on the growth rates. Complementary measurements on thicker films, which contained fewer holes per unit area [107], showed that this initial (most likely) exponential growth regime passed over to a slower behavior at hole diameters below 1 μm, coinciding with the appearance of a rim.

During the subsequent stages of visco-elastic dewetting, a rim developed and its shape changed significantly over time. Initially, the energy supplied by the driving forces was mainly dissipated within the volume of the film in the vicinity of the hole (via deformations in the radial and ortho-radial). The removed material (related to the dewetted distance d) was redistributed within the film over a certain distance Δ_0, which is characterized by film thickness h_0 and frictional properties [42, 46, 144]:

$$d \ll \Delta_0 \sim (h_0 \eta / \zeta)^{1/2} \tag{14}$$

with ζ being the friction coefficient at the interface and η the viscosity of the film. Under such conditions, no rim was formed next to the circular dewetted zone.

However, as the radius of the hole becomes larger than Δ_0, this contribution to dissipation becomes smaller compared to friction at the substrate–film interface. As a consequence of such friction, the velocity is damped over the distance Δ_0 within

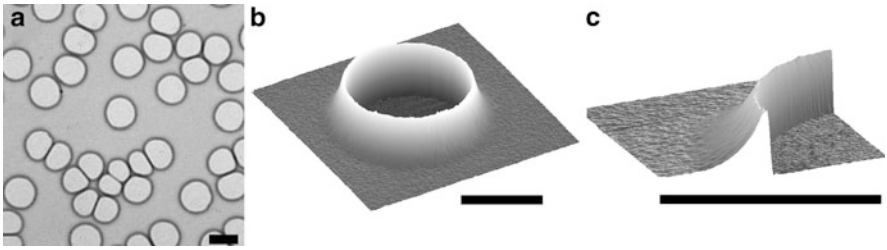

Fig. 14 Typical examples of holes and the corresponding rim formed in a 24-nm thick PS film. This film is thick enough for holes to be separated by several micrometers on average. (**a**) Optical micrograph after annealing for 80 min at 120°C. AFM images (**b**) and (**c**) focus on the asymmetric shape of the rim. Scale bars: 5 μm

the film. This damping results in the appearance of a highly asymmetric rim (Fig. 14), with a steep side reaching a height H next to the three-phase contact line and an approximately exponential decay on the other side, with a decay length Δ_0 [17, 42, 44].

The highly asymmetric shape of the rim suggests that the polymer does not flow like a liquid. For a viscous fluid we would expect that equilibration of the Laplace pressure (which is proportional to curvature) within the rim is fast, i.e., fast with respect to the shortest possible experimental time scale. This would lead to a more symmetric shape. In our experiments, the asymmetric shape of the rim represents a characteristic feature of dewetting of high molecular weight visco-elastic fluids at temperatures close to T_g [17, 37, 38, 41–48]. Typical examples showing the evolution of the shape of the rim are given in Fig. 15.

The change in shape of the rim with time can be followed by taking cross-sections through holes after different annealing times (Fig. 16). At the very beginning of hole formation (for hole diameters less than about 1 μm), no rim could be detected (see the smallest hole diameter in Fig. 16). As the holes became larger, the build-up of the highly asymmetric rim could be followed. Interestingly, the maximum height of the rim increased almost linearly with time.

The decay on the rear side can be fitted to an exponential function $y = A \exp[(x - x_0)/\Delta_0] + y_0$ with amplitude A and offsets x_0 and y_0. As expected by theory [42, 44, 46, 47], the characteristic decay length Δ_0 did not vary with annealing time. Fits to the profiles shown in Fig. 16 all resulted in $\Delta_0 \sim 0.5$ μm. We note, however, that Δ_0 could vary between 0.3 μm and several micrometers for samples with slightly varying thicknesses of the PDMS coating. The hole opening velocity was faster for larger Δ_0.

As in dewetting experiments with simple (Newtonian) fluids, one can also measure the width w of the rim. To do this, the exponential decay is truncated when the height of the rim (measured from the substrate level) has decayed to a value about 1.1 h_0. Then, according to theory [42, 44, 46, 47], $w = \sqrt{2}\,\Delta_0 \ln(10t/\tau)$, with τ being a characteristic relaxation time of the polymer. As can be seen in

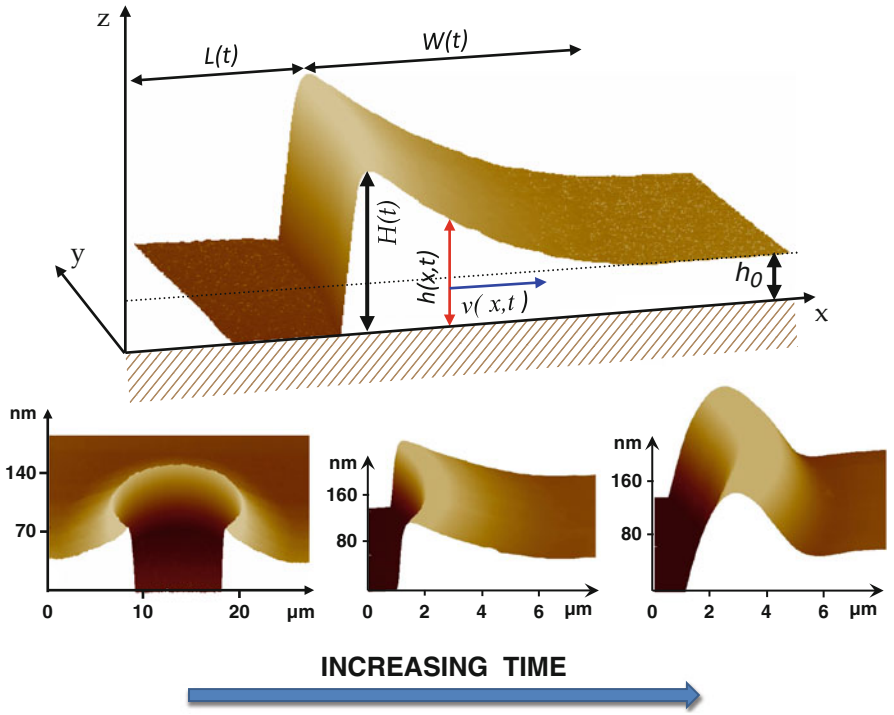

Fig. 15 *Top*: 3D view (measured by AFM) of a typical hole obtained by dewetting a PS film on a PDMS-coated substrate at temperatures close to the glass transition of PS. $h(x,t)$ is the profile of the film, h_0 is the initial height of the film, $H(t)$ is the height of the front, $L(t)$ is the dewetted distance, $W(t)$ is the width of the rim, and $v(x,t)$ is the velocity of the film. *Bottom*: typical 3D cross-sections showing the asymmetric shape of the rim at early stages and comparatively low temperatures (*left*) and the more symmetric shape at late stages or at high temperatures (*right*)

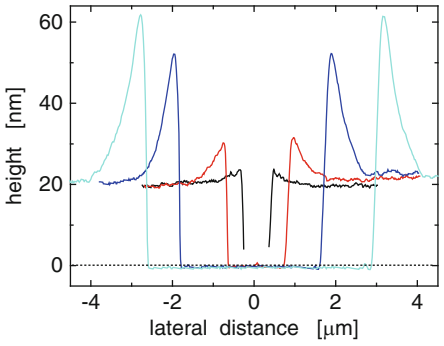

Fig. 16 Cross-sections through holes and surrounding rims of highly asymmetric shape formed in a 20-nm thick PS film after annealing for 1, 5, 40, and 80 min at 120°C

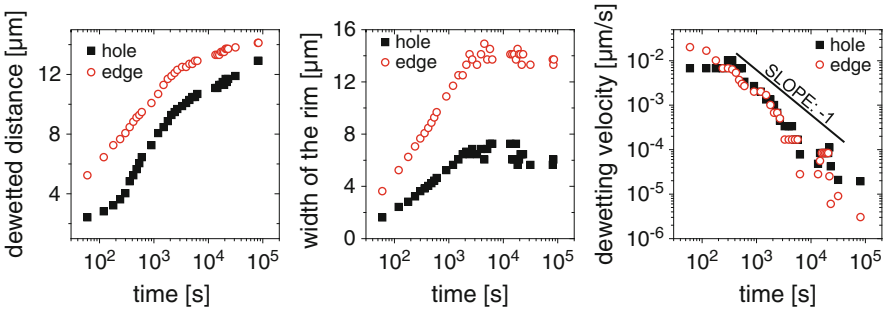

Fig. 17 Results of a typical dewetting experiment for high molecular weight PS film. A 55-nm thick film ($M_w = 4{,}840$ kg/mol) was dewetted at 130°C on a silicon wafer coated with an adsorbed PDMS layer ($M_w = 139$ kg/mol). The growth of a nucleated hole is compared to dewetting from a straight edge, established by breaking the silicon wafer into two parts

Fig. 17, during the early stages of rim build-up, both the dewetted distance, d, and the width of the rim, w, increased in a logarithmic fashion in time, up to a time τ_w when w reached a maximum (w_{max}). At times larger than τ_w, the width of the rim either remained constant or decreased. τ_w can also be related to a transition of the highly asymmetric rims to more symmetric ones. During this early stage of rim build-up and even at times larger than τ_w, the dewetting velocity V decreased continuously according to a power law, $V \sim t^{-1}$. We note that, besides differences at very short times, the opening of a hole and the retraction from a straight line like the edge of the sample yielded similar dewetting kinetics (see Fig. 17).

We want to emphasize that a logarithmic time dependence of d and w, and the corresponding t^{-1} decrease of V, are not expected for a Newtonian liquid [42]. Moreover, our results cover times shorter than the longest relaxation time in equilibrated bulk samples (i.e., the reptation time). Thus, the visco-elastic properties of PS certainly affect our dewetting experiments. Thus, a detailed theoretical model has been developed that takes into account residual stresses, interfacial friction (i.e., slippage), and visco-elasticity [42, 44, 46].

In Fig. 18, we show the results of dewetting experiments performed at different temperatures and for two polymers of different lengths. w always increased approximately logarithmically in time until it reached a maximum value at τ_w. In equilibrated bulk samples, the existence of entanglements implies that the longest relaxation times (i.e., the reptation time τ_{rep}) strongly depends on molecular weight, M_w according to a power law, $\tau_{rep} \sim M_w^{3.4}$ [163, 164]. Moreover, the temperature dependence of the relaxation time follows a non-Arrhenius behavior when approaching T_g. The thermal evolution of relaxation times is usually described by the Vogel–Tamman–Fulcher (VTF) relation [163, 164], $\tau = \tau_0 \exp[B/(T - T_0)]$, with the material-dependent characteristic temperature $B = 1{,}170$ K and $T_0 = 343$ K for bulk PS [163, 164]. Interestingly, for the longer polymer, τ_w was drastically shorter than τ_{rep}.

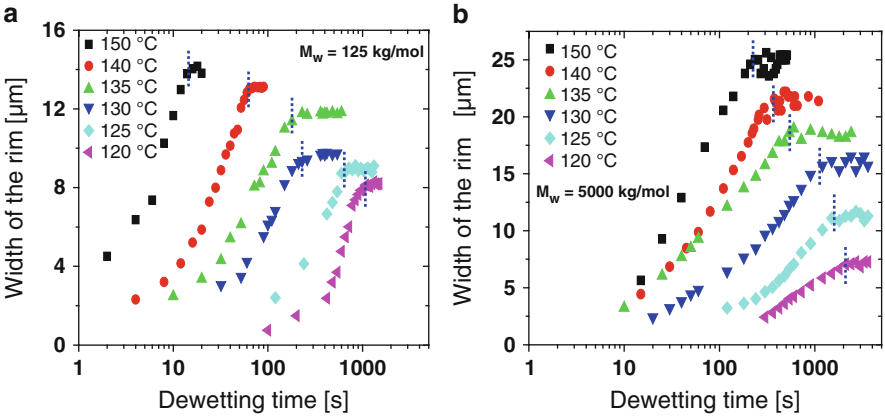

Fig. 18 Temporal evolution of the width w of the rim of holes growing in thin PS films of (**a**) $M_w = 125$ kDa and (**b**) $M_w = 5{,}000$ kDa as a function of dewetting time at various temperatures, as indicated. Relaxation time τ_w is determined by the time when the width of the rim reaches its maximum, as indicated by the *dotted lines*

In Fig. 19, we present a comparison of the values of τ_w for polymers of different chain lengths as a function of temperature. The shorter chains approximately followed a VTF behavior [163, 164] with the values of τ_w and τ_{rep} being almost identical at high temperatures. However, the longer polymers showed significant deviations from such behavior. At the lowest temperatures, we did not observe any influence of molecular weight. The values of τ_w were almost identical for all polymers studied. At higher temperatures τ_w varied only slightly with temperature, much less than expected from a VTF behavior. In addition, all values of τ_w were several orders of magnitude lower than τ_{rep} of these long chain polymers in the bulk.

The evolution of τ_w with molecular weight showed striking deviations from bulk behavior. For high molecular weights, we observed that the relaxation time τ_w, as determined from a w_{max} versus time plots, became almost independent of the chain length (Fig. 20).

For low M_w, this relaxation was clearly related to the reptation time, τ_{rep}, suggesting that this relaxation process is dominated by the mobility of whole chains. In contrast, for high M_w above about 300 kDa, very large deviations with respect to bulk reptation times were observed, suggesting that the corresponding relaxation process only requires the motion of a part of such long chains. For the longest chains studied, we found $\tau_w \ll \tau_{rep}$ by several orders of magnitude. The most striking feature is that almost the same value of τ_w was obtained for polymers of very different lengths.

Above results clearly demonstrate that dewetting can be considered as a "nano-rheology" experiment that gives insight into the structure and properties of out-of-equilibrium PS thin films. We may thus consider dewetting as a rheological "probe" for the study of the visco-elastic properties of nanoscopic polymer films.

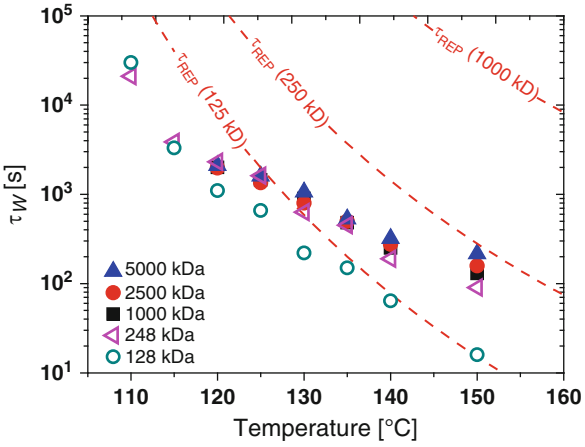

Fig. 19 Evolution of the relaxation time τ_w (deduced from the position where the width of the rim reached a maximum value) as a function of dewetting temperature for PS of different molecular weights. Evolution of bulk reptation times is indicated by *dashed lines*. The film thickness was set at 40 nm

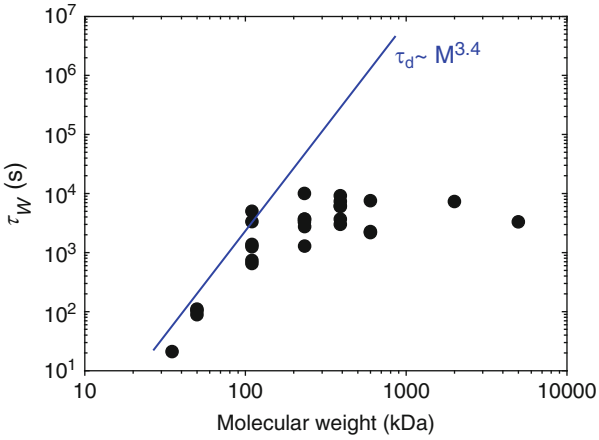

Fig. 20 Evolution of the relaxation time τ_w (deduced from the width of the rim and the dewetting dynamics) as a function of molecular weight together with the evolution of bulk reptation times. τ_d is the reptation time representing the longest relaxation time of a polymer of molecular weight M. The film thickness was set at 100 nm

We tentatively interpret τ_w as the time needed to relax chain conformations, which were trapped in strongly out-of-equilibrium states. These conformations were generated by rapid solvent evaporation in the course of film preparation [17, 37–48] because the chains were rather diluted in solution and did not have sufficient time to establish the equilibrium state during the process of spin-coating.

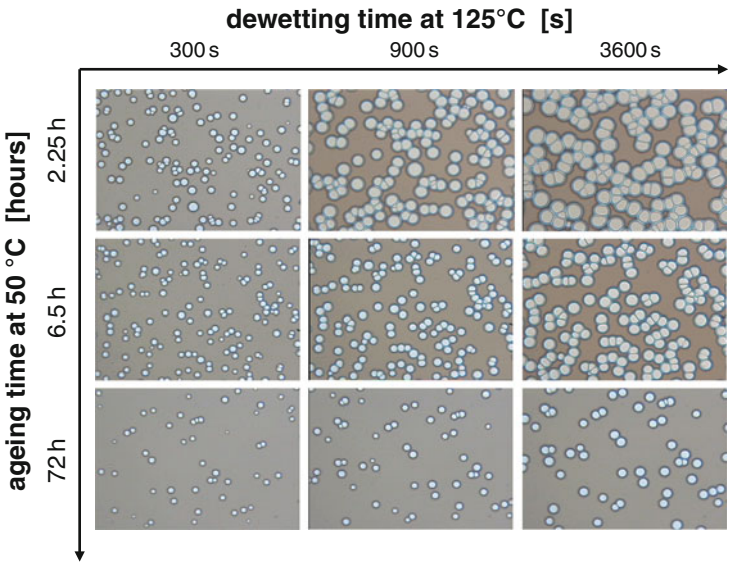

Fig. 21 Influence of ageing PS films at 50°C on the probability of film rupture when annealing (and consequently dewetting) at 125°C. Clearly, the number of holes and the diameter at a given time of dewetting decrease with ageing time. The size of the images is 310 μm × 210 μm

We anticipate that the entanglement density in the dry spin-coated films is lower than in an equilibrated bulk system. Such a departure from equilibrium most likely generates residual stresses. As one consequence, we tentatively attribute the observed hole nucleation, which initiated the dewetting process of holes, to the presence of such residual stresses within the film [165]. In this way, rupture can be related to the spin-coating process used to prepare thin polymer films.

One may ask if these residual stresses are (partially) relaxing even in the glassy state of the film. Thus, we varied systematically the duration for which such films were stored below T_g. As a first phenomenon, we focused on the process of film rupture. In a second stage, we also studied the early stages of the dewetting dynamics. In Fig. 21, we present some typical results for PS films of high molecular weight polymers aged at 50°C for various times. As can be seen already from these micrographs, these two independent processes of rupture and dewetting proved equally and in parallel the significance of residual stresses and indicated that these stresses relaxed upon aging. The older the films were, the fewer holes were formed and the slower was the dewetting process.

The presence of residual stresses in polymer thin films can thus be considered as an explanation for the rupture mechanism via heterogeneous nucleation. We have found that the probability for film rupture, defined as the maximum number N_{max} of circular holes per unit area formed in a film of given thickness, also depended on ageing time, the time the film was stored at temperatures below T_g [17]. It should be noted that ageing of the films started at the time of the solvent quench during

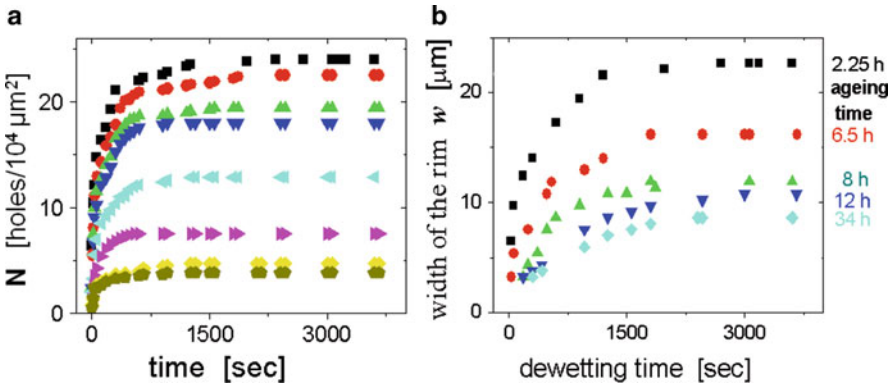

Fig. 22 Influence of ageing on the probability of film rupture, expressed via the number of holes per unit area (N). (**a**) N as a function of time at 125°C for PS films ($h_0 = 40$ nm, $M_w = 4{,}840$ kg/mol) after being aged at 50°C for increasing times (from *top* to *bottom*: 2.25, 6.5, 8, 12, 34, 72, 108, and 134 h). The maximum value N_{max} (per 10^4 µm^2) for each sample is reached within about 100 s. (**b**) Temporal evolution of the width w of the rim of holes growing in these films after various ageing times at 50°C, as indicated. The maximum value w_{max} was reached after about 2,000 s and clearly decreased with ageing time

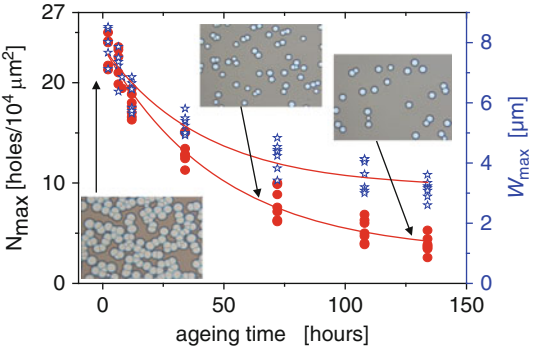

Fig. 23 Systematic study of N_{max} (*circles*) and w_{max} (*stars*) for the same type of films as in Fig. 22, stored at 50°C for various times. The *insets* show some typical corresponding optical micrographs (310 µm × 230 µm). The *solid lines* represent the fit to an exponential function. The exponential behavior of N_{max} is comparable to the exponential decrease in the maximum width of the rim (w_{max}) with aging time

spin-coating. As can be seen in Figs. 21, 22, and 23, a drastic reduction in hole density was observed after storing the films at 50°C for increasingly longer times.

The maximum number of holes (N_{max}) as a function of ageing time (Fig. 23) can be described by an exponential decay with ageing time t_{ageing}, such that $N_{max}(t_{ageing}) = N_{max}(\infty) + N_{max}(0)\cdot\exp[-t_{ageing}/\kappa(N_{max})]$, with a limiting value $N_{max}(\infty) = 3 \pm 1$ and a characteristic decay-time $\kappa(N_{max}) = 47 \pm 6$ h, implying that almost no holes

will be formed after ageing the films for extended periods ($t_{ageing} \gg \kappa$). Some holes, however, may be nucleated by defects like dust particles.

Analogous to the initial rupture probability of the films (see Fig. 21), physical ageing at temperatures below T_g also drastically influenced the dewetting dynamics [17]. Figure 22b shows that the maximum width of the rim, w_{max}, and the dewetting velocity (not shown) decreased significantly when the films were aged. Measurable ageing effects could be achieved even at room temperature [17], i.e., 75°C below T_g. For example, after storing films for 42 days at room temperature, w_{max} decreased by a factor of 2. Systematic studies on the temporal evolution of w_{max} for films stored at 50°C (Fig. 22) showed an exponential decay of w_{max} with ageing time t_{ageing}, such that $w_{max}(t_{ageing}) = w_{max}(\infty) + w_{max}(0)\cdot\exp[-t_{ageing}/\kappa(w_{max})]$, exhibiting a characteristic decay time $\kappa(w_{max}) = 41 \pm 7$ h, very close to the decay time observed for hole nucleation probability.

The large decrease in dewetting velocity observed during ageing at temperatures well below T_g of PS can be interpreted by considering either a decrease in residual stress or a modification (in the course of ageing) of the PS–PDMS interface, and thus of the friction properties. Theoretically, the contribution of residual stresses to the dewetting dynamics is equivalent to an additional driving force, in parallel to the capillary forces. This additional force will decrease during dewetting. Relaxation of residual stresses during physical ageing also causes a reduction in the driving force. Residual stresses σ lead to an increase of the initial dewetting velocity by a factor $(1 + h_0\sigma/|S|)$, with S being the spreading factor given by $S = \gamma_{sv} - \gamma_{sl} - \gamma_{lv} \sim 10^{-2}$ N/m^2, where γ_{sv}, γ_{sl}, and γ_{lv} are the solid–vapor, solid–liquid, and liquid–vapor surface energies, respectively [42].

Based on the assumption that the relaxation of the rim shape can be directly related to the relaxation of the residual stress [42, 44, 46], we conclude that a significant fraction of residual stress could be relaxed via limited motions of parts of the polymer chain. It should, however, be noted that even after τ_w, the conformations of long chains probably still remain out-of-equilibrium, i.e., part of the residual stresses may relax without fully equilibrating the polymers.

The dewetting dynamics of such visco-elastic thin films can be described by a Jeffrey rheological model considering G the elastic modulus (mainly due to chain entanglements), η_0 a short time viscosity and η_1 the melt viscosity [42–47, 164]. The relaxation times of the fluid are given by $\tau_{0,1} = \eta_{0,1}/G$ (the longest relaxation time, τ_1 can be compared to the reptation time of the chains). The time response of such a fluid can thus be divided into three regimes. At short or long times ($t < \tau_0$ or $t > \tau_1$), the liquid behaves like a simple Newtonian liquid with small (η_0) or large (η_1) viscosity, respectively. For the intermediate regime, however, the liquid behaves like an elastic solid of modulus G. At times longer than the reptation time, the polymer chains started to flow as a viscous fluid of high viscosity and thus the dewetting velocity decreases as described by the classical power law related to viscous dewetting on slippery substrates, $V \sim t^{-1/3}$ [112, 144].

In the case of dewetting of purely elastic films, the height of the rim can only reach a well-defined maximum height H_{max}. Assuming that only capillary stress (S/h_0) is acting at the contact line, we obtain: $H_{max} - h_0 \sim S/G$. Mass conservation

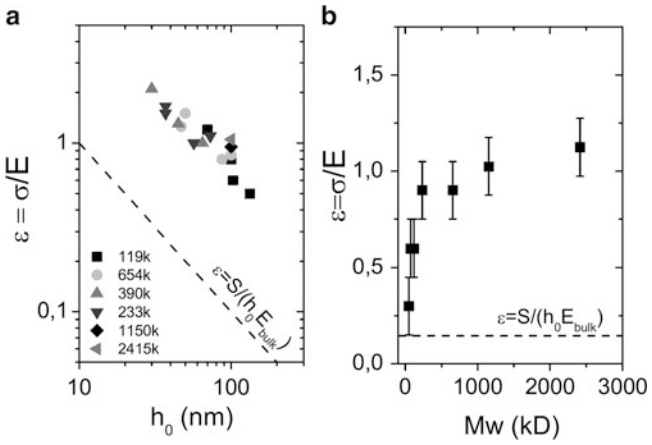

Fig. 24 Evolution of the strain, $\varepsilon = (H - h_0)/h_0$, determined from the plateau value of a plot of the height increase $(H - h_0)$ versus the width of the rim (w), with (**a**) film thickness (M_w as indicated) and (**b**) molecular weight ($h_0 \sim 100$ nm). The *dashed line* in both graphs corresponds to the strain that would be expected for equilibrated PS films: $\varepsilon = S/(h_0\, E_{bulk})$ (adapted from [25])

imposes an augmentation of the rim width during the dewetting process: $d{\cdot}h_0 \sim w{\cdot}(H_{max} - h_0)$ [17, 43, 45], which finally yields the relations $H_{max} - h_0 \sim d/w{\cdot}h_0$ and $w = d{\cdot}h_0{\cdot}G/|S|$. Thus, the rim height can be determined from the rim width, w, and the dewetted distance, d, by considering the mass conservation.

For the time regime $\tau_0 > t > \tau_{rep}$, we expect a drastic influence of elasticity on rim formation. The strain, ε, can be easily deduced from the width of the rim, w, and the dewetted distance, d. We obtain: $\varepsilon = (H - h_0)/h_0 \sim 2d/w$. This relation between d, w, and H, and thus ε, was confirmed by AFM [43]. As shown in [43], the rim height first increases continuously with the rim width up to its maximum value, in agreement with the theoretical model proposed by Vilmin and Raphaël [42].

In the above presented experiments, the deformation of the elastic polymer (for times much shorter than the reptation time, a polymer behaves essentially like an elastic body) is given by the relation $\varepsilon = \sigma/E = (\sigma_{cap} + \sigma_{res})/E$. The strain, ε, is thus determined by the capillary stress at the edge of the film ($\sigma_{cap} = S/h_0$), the residual stress, σ_{res}, and the elastic modulus, E. For a PS film with equilibrated, fully entangled chain conformations ($G \sim 1$ MPa) and without residual stress, ε is determined only by the capillary stress and is consequently very small, $\varepsilon \sim S/(h_0 E) \sim 0.1$, which is almost negligible in comparison with the high strains observed in the experiments represented in Fig. 24.

Several points need to be emphasized. High strains were observed even for film thicknesses much larger than the unperturbed dimension of the chains represented by the end-to-end distance of the polymer coils (R_{ee}). Thus, chain confinement can be ruled out as the cause for high values of ε.

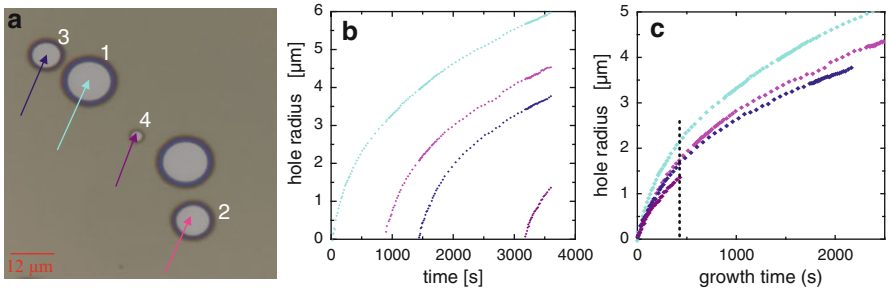

Fig. 25 Growth of typical dewetting holes in a 45-nm thick PS film was followed by optical microscopy. (**a**) The four holes marked *1–4* were nucleated after an incubation time of 20, 900, 1,440, and 3,180 s, respectively, after the film was brought to 125°C. (**b**) The radius of each hole (*1–4* are shown from *top* to *bottom*, respectively) is plotted as a function of the time the film was incubated at 125°C. (**c**) The ordinate is rescaled to the time that each hole had grown since it was nucleated, rather than the time elapsed since the film reached 125°C

As ε is given by the ratio σ/E, the explanation of high values of ε may be linked to both large residual stresses and/or small elastic modulus. Both consequences leading to high values of ε can be related to the preparation of the films by spin-coating.

The above experiments clearly point out that residual stresses can be introduced by rapid solvent loss during spin-coating, most likely caused by out-of-equilibrium chain conformations [42–46]. Consequently, the dewetting behavior reflects viscoelastic properties deviating from bulk [46]. However, at present, it is not clear how such chain conformations depend on the properties of the solution and on the solution-to-glass transition. Neither is it clear how the resulting mechanical and relaxation properties depend on the preparation stage. Thus, based on the well-supported hypothesis that film preparation introduces non-equilibrium chain conformations, we now focus on the influence of properties of the solution used for spin-casting by varying the solution temperature [48]. By increasing the temperature of the solution, we varied the radius of gyration from proportional to $N^{1/2}$ for a near-Θ solution to $N^{0.588}$ for good solvent conditions (N is the number of monomers per chain). To this end, we used *trans*-decalin (TD) which is a solvent for PS and has a Θ-temperature of about 21°C. The degree of swelling of PS chains in the solution could be varied over a considerable range [166]. For the long chain polymer used ($M_w = 4{,}060$ kDa), the coil radius changes by about 40% when changing the temperature from 21°C to 55°C. We first study the dewetting dynamics for a 45-nm thick PS film prepared at 23°C. When brought to $T = 125°C > T_g$, the holes nucleated after various incubation times (see Fig. 25). Such a gradual nucleation of holes allowed direct comparison of holes having experienced different thermal history. Holes that nucleated at later times exhibited a slower opening rate.

A comparison of the hole radius (measured at a constant growth time of 430 s) indicates an exponential relaxation (see Fig. 26), yielding a decay time of about 30 min for the hole-opening driving force.

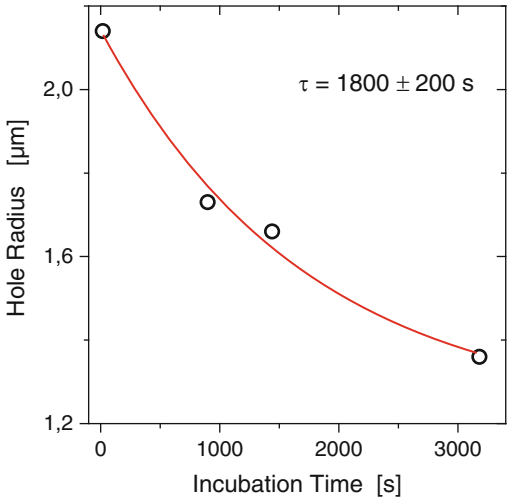

Fig. 26 Hole radius after a growth time of 430 s (*vertical dotted line* in Fig. 25c) as a function of incubation time. τ decay time

This dependence of hole radius on incubation time clearly demonstrates relaxation processes within the film even in the course of dewetting. Note that the differences in hole opening behavior were observed in a single sample and almost simultaneously.

The relaxation process may lead either to a decrease in residual stress or an increase in elastic properties, or both, with incubation time. However, independent of the actual interpretation, these results support the hypothesis that the chains in the films, which were initially out of equilibrium, tend to equilibrate during annealing. As shown above, this relaxation process was documented by dewetting. Interestingly, relaxations were much faster than according to bulk reptation at 125°C for the high molecular weight PS used here ($\tau_{rep} \sim 2 \times 10^8$ s) [43, 104, 163, 164].

In a second series of experiments, films spin-cast from TD at 25°C were aged at room temperature for various times before being heated to 125°C for dewetting measurements. Only holes nucleated immediately upon reaching 125°C were considered. Figure 27 displays characteristic results for the hole-opening kinetics for films with increasing aging time. The hole radii of these six samples at three fixed hole-opening times show an exponential decay, defining an almost identical characteristic relaxation time of the film of 43 ± 9 h. Note that a comparison between samples aged in ambient atmosphere and in vacuum showed no difference in dewetting behavior, excluding an effect of residual solvent in the film.

Additional samples made from solutions of varying solvent quality, i.e., films that were spin-cast from TD at different temperatures, were also aged at room temperature and analyzed in terms of their hole radius or dewetting velocity as a function of dewetting time. Varying the temperature of the spin-coating solution has a substantial effect on the room temperature relaxation process of these films spun from TD solutions (see Fig. 28), corresponding to a change in relaxation times

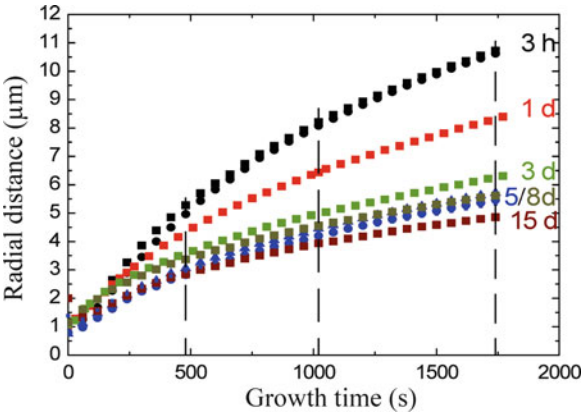

Fig. 27 Growth of dewetting holes nucleated immediately upon heating to 125°C in films cast from TD at 25°C that had been aged at room temperature for the times indicated. Holes exhibit decreasing growth velocities with increasing ageing time. Hole radii taken at three constant times (480, 1,020 and 1,740 s, indicated by the vertical *dashed lines*) follow an exponential decay with a characteristic time of 43 ± 9 h, reflecting a relaxation process of chain segments within the film at room temperature, i.e., in the glassy state

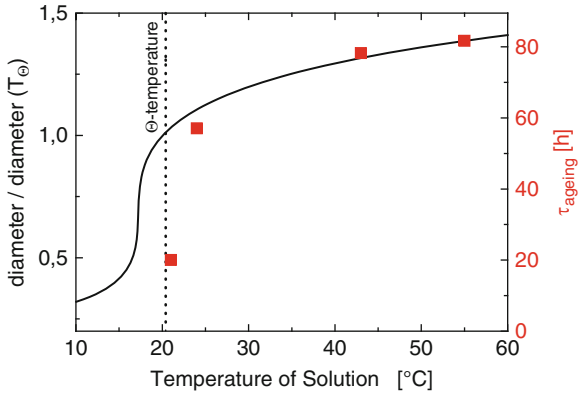

Fig. 28 Relaxation time τ_{ageing} *(squares)* as a function of temperature of the solution from which the films were spun. The *solid line* represents the coil diameter of the individual polymer in solution, normalized by its diameter at the Θ temperature of PS in *trans*-decalin (indicated by the vertical *dotted line*)

by a factor of 4. In comparison, films cast from toluene (at room temperature) had a relaxation time of ~700 h at room temperature, in agreement with the extrapolation of Fig. 28 to the athermal limit (i.e., a relative coil diameter of 2.5).

A decrease in dewetting velocity with increased aging time is indicative of a decaying stress or an increasing modulus with aging time of the sample. Figure 28

indicates that the relaxation time determined from dewetting experiments on aged samples follows a similar trend with temperature as does the coil diameter in solution. Thus, we may tentatively conclude that more compact chains in solution at lower temperatures allow only the formation of a lower number of entanglements with other chains. Consequently, these more weakly entangled polymers yield a lower film modulus and allow a faster relaxation process in the glassy state at room temperature.

5 Conclusions

The examples presented here clearly demonstrate the potential of dewetting studies for the investigation of properties of thin polymer films. The main advantage of the dewetting approach is its simplicity in obtaining complementary information on the relation between the molecular scale interfacial properties and macroscopic behavior, both static and kinetic. Using a Newtonian fluid as a model system allowed us to verify that the underlying physics of the dewetting process is well understood.

Applying this approach to spin-coated glassy PS films opens up several interesting possibilities for the study of visco-elastic properties and relaxation processes in such films. In particular, significant deviations from bulk behavior could be identified for films of high molecular weight. Moreover, dewetting also indicates that the conformation of chains in the initial solution has a great impact on the behavior of resultant dry films due to the out-of-equilibrium states that are frozen-in by spin-coating. In general, dewetting experiments are able to demonstrate the role of the non-equilibrium conformation of the chains in the film. Our data on films aged at room temperature suggest a variation in quenched chain entanglements that depends on the solvent quality from which the film was cast. We see that the quality of the solvent and the history of the solution up to the point of vitrification, not just the thermal history of the film after vitrification, must be taken into account to predict the behavior of polymeric thin films.

The strong dependence of film preparation conditions on the aging behavior of thin films far below T_g and the observation of significant changes even at room temperature may also be of relevance in the context of the low "softening" temperature of thin polymer films, typically interpreted as a reduced T_g. While the deformation of polymer coils as a whole should not modify the solidification temperature of the film, which is dominated by the segmental dynamics, our aging experiments indicate that spin-coating perturbs the polymer coils down to the segmental length scale. At present, it is not clear if and how our observations using dewetting can be reconciled with a lowered T_g. Thus, further experiments are needed to verify whether non-equilibrium chain conformations induced, e.g., by film preparation can explain all anomalous properties of thin polymer films, such as deviations from T_g in the bulk.

Acknowledgments I am highly indebted to Françoise Brochard and the late Pierre-Gilles de Gennes for many invaluable discussions. I wish to thank Rajesh Khanna, Samer Al Akhrass, Pascal Damman, Mithun Chowdhury, Ulli Steiner, Adam Raegen, Thomas Vilmin, Falko Ziebert, and Elie Raphaël for the fruitful collaborations which are at the base of the results presented here. I am grateful to the Deutsche Forschungsgemeinschaft (RE2273/3-1) for funding of the most recent part of this work and partial financial support from the European Community's "Marie-Curie Actions" under contract MRTN-CT-2004-504052 [POLYFILM] for the earlier stage of the work.

References

1. Reiter G (1993) Europhys Lett 23:579–584; (1994) Macromolecules 27:3046–3052
2. Orts WJ, van Zanten JH, Wu WL, Satija SK (1993) Phys Rev Lett 71:867–870
3. Sanyal MK, Basu JK, Datta A, Banerjee S (1996) Europhys Lett 36:265–270
4. Reiter G, de Gennes PG (2001) Eur Phys J E 6:25–28
5. Mukherjee M, Bhattacharya M, Sanyal MK, Geue T, Grenzer J, Pietsch U (2002) Phys Rev E 66:061801
6. Bhattacharya M, Sanyal MK, Geue T, Pietsch U (2005) Phys Rev E 71:041801
7. Kanaya T, Miyazaki T, Watanabe H, Nishida K, Yamana H, Tasaki S, Bucknall DB (2003) Polymer 44:3769–3773
8. Miyazaki T, Nishida K, Kanaya T (2004) Phys Rev E 69:022801
9. Richardson H, Lopez-Garcia I, Sferrazza M, Keddie JL (2004) Phys Rev E 70:051805
10. Bollinne C, Cuenot S, Nysten B, Jonas AM (2003) Eur Phys J E 12:389–395
11. Tsui OKC, Russell TP (2008) Polymer thin films. World Scientific, Singapore
12. Tsui OKC, Wang YJ, Lee FK, Lam CH, Yang Z (2008) Macromolecules 41:1465–1468
13. Dalnoki-Veress K, Nickel B, Roth C, Dutcher J (1999) Phys Rev E 59:2153–2156
14. Akabori K-I, Tanaka K, Kajiyama T, Takahara A (2003) Macromolecules 36:4937–4943
15. Kawana S, Jones RAL (2003) Eur Phys J E 10:223–230
16. Priestley RD, Broadbelt LJ, Torkelson JM (2005) Macromolecules 38:654–657
17. Reiter G, Hamieh M, Damman P, Sclavons S, Gabriele S, Vilmin T, Raphael E (2005) Nat Mater 4:754–758
18. Lee H, Paeng K, Swallen S, Ediger M (2008) J Chem Phys 128:134902
19. Fukao K, Koizumi H (2008) Phys Rev E 77:021503
20. Priestley RD (2009) Soft Matter 5:919–926
21. Pye JE, Rohald KA, Baker EA, Roth CB (2010) Macromolecules 43:8296–8303
22. Brown HR, Russell TP (1996) Macromolecules 29:798–800
23. Herminghaus S, Jacobs K, Seemann R (2001) Eur Phys J E 5:531–538
24. Efremov M et al (2003) Phys Rev Lett 91:085703
25. Fakhraai Z, Forrest JA (2005) Phys Rev Lett 95:25701
26. Fakhraai Z, Valadkhan S, Forrest JA (2005) Eur Phys J E 18:143
27. Fakhraai Z, Forrest JA (2008) Science 319:600–604
28. Rathfon JM, Cohn RW, Crosby AJ, Tew GN (2011) Macromolecules 44:134–139
29. Jones R, Kumar S, Ho D, Briber R, Russell TP (1999) Nature 400:146–149
30. Brulet A, Boue F, Menelle A, Cotton JP (2000) Macromolecules 33:997–1001
31. Kraus J, Müller-Buschbaum P, Kuhlmann T, Schubert D, Stamm M (2000) Europhys Lett 49:210–216
32. Si L, Massa MV, Dalnoki-Veress K, Brown HR, Jones RAL (2005) Phys Rev Lett 94:127801
33. Reiter G, Schultz J, Auroy P, Auvray L (1996) Europhys Lett 33:29
34. Debregeas G, de Gennes PG, Brochard-Wyart F (1998) Science 279:1704–1707
35. Reiter G (2001) Phys Rev Lett 87:186101
36. Reiter G (2002) Eur Phys J E 8:251–255

37. Damman P, Baudelet N, Reiter G (2003) Phys Rev Lett 91:216101
38. Gabriele S, Sclavons S, Reiter G, Damman P (2006) Phys Rev Lett 96:156105
39. Bodiguel H, Fretigny C (2006) Eur Phys J E 19:185–193
40. Yang MH, Hou SY, Chang YL, Yang ACM (2006) Phys Rev Lett 96:066105
41. Gabriele S, Damman P, Scalvons S, Desprez S, Coppée S, Reiter G, Hamieh M, Al-Akhrass S, Vilmin T, Raphaël E (2006) J Polym Sci B Polym Phys 44:3022
42. Vilmin T, Raphaël E (2006) Eur Phys J E 21:161
43. Damman P, Gabriele S, Coppee S, Desprez S, Villers D, Vilmin T, Raphael E, Hamieh M, Al-Akhrass S, Reiter G (2007) Phys Rev Lett 99:036101
44. Vilmin T, Raphaël E, Damman P, Sclavons S, Gabriele S, Hamieh M, Reiter G (2006) Europhys Lett 73:906
45. Reiter G, Al Akhrass S, Hamieh M, Damman P, Gabriele S, Vilmin T, Raphael E (2009) Eur Phys J ST 166:165–172
46. Ziebert F, Raphaël E (2009) Phys Rev E 79:031605
47. Ziebert F, Raphael E (2009) Europhys Lett 86:46001
48. Raegen A, Chowdhury M, Calers C, Schmatulla A, Steiner U, Reiter G (2010) Phys Rev Lett 105:227801
49. Coppée S, Gabriele S, Jonas A, Jestin J, Damman P (2011) Soft Matter 7:9951
50. Richardson H, Carelli C, Keddie J, Sferrazza M (2003) Eur Phys J E 12:437–441
51. Chung JY, Chastek TQ, Fasolka MJ, Ro HW, Stafford CM (2009) ACS Nano 3:844–852
52. Barbero DR, Steiner U (2009) Phys Rev Lett 102:248303
53. Thomas KR, Chenneviere A, Reiter G, Steiner U (2011) Phys Rev E 83:021804
54. Thomas K, Steiner U (2011) Soft Matter 7:7839
55. Keddie JL, Jones RAL, Cory RA (1994) Europhys Lett 27:59
56. Forrest JA, Dalnoki-Veress K, Stevens JR, Dutcher JR (1996) Phys Rev Lett 77:2002–2005
57. Forrest JA, Dalnoki-Veress K, Dutcher JR (1997) Phys Rev E 56:5705–5716
58. Prucker O, Christian S, Bock H, Rühe J, Frank CW, Knoll W (1998) Macromol Chem Phys 199:1435–1444
59. Forrest JA, Mattsson J (2000) Phys Rev E 61:R53–R56
60. Forrest JA, Dalnoki-Veress K (2001) Adv Coll Interf Sci 94:167
61. van der Lee A, Hamon L, Holl Y, Grohens Y (2001) Langmuir 17:7664–7669
62. Dalnoki-Veress E, Forrest JA, Murray C, Gigault C, Dutcher JR (2001) Phys Rev E 63:031801
63. Tsui OKC, Zhang HF (2001) Macromolecules 34:9139–9142
64. Reiter G, Forrest J (2002) Special issue on properties of thin polymer films. Eur Phys J E 8:101
65. Grohens Y, Hamon L, Spevacek J, Holl Y (2003) Macromol Symp 203:155–164
66. Ellison CJ, Torkelson JM (2003) Nat Mater 2:695–700
67. Soles CL, Douglas JF, Wu WL, Peng HG, Gidley DW (2004) Macromolecules 37:2890–2900
68. Soles CL, Douglas JF, Jones RL, Wu WL (2004) Macromolecules 37:2901–2908
69. Ellison CJ, Ruszkowski RL, Fredin NJ, Torkelson JM (2004) Phys Rev Lett 92:095702
70. O'Connell PA, McKenna GB (2005) Science 307:1760
71. Alcoutlabi M, McKenna GB (2005) J Phys Condens Matter 17:R461–R524
72. Priestley RD, Ellison CJ, Broadbelt LJ, Torkelson JM (2005) Science 309:456–459
73. Lupascu V, Picken SJ, Wübbenhorst M (2006) Macromolecules 39:5152–5158
74. Peter S, Meyer H, Baschnagel J (2006) J Polym Sci B Polym Phys 44:2951–2967
75. Napolitano S, Wübbenhorst M (2007) J Phys Chem B 111:5775–5780
76. Napolitano S, Wübbenhorst M (2007) J Phys Chem B 111:9197–9199
77. Napolitano S, Prevosto D, Lucchesi M, Pingue P, D'Acunto M, Rolla P (2007) Langmuir 23:2103–2109
78. Napolitano S, Lupascu V, Wübbenhorst M (2008) Macromolecules 41:1061–1063
79. Yang ZH, Wang YJ, Todorova L, Tsui OKC (2008) Macromolecules 41:8785–8788
80. Serghei A, Kremer F (2008) Macromol Chem Phys 209:810–817

81. Peter S, Napolitano S, Meyer H, Wübbenhorst M, Baschnagel J (2008) Macromolecules 41:7729–7743
82. Kim S, Hewlett SA, Roth CB, Torkelson JM (2009) Eur Phys J E 30:83–92
83. Rotella C, Napolitano S, Wübbenhorst M (2009) Macromolecules 42:1415–1417
84. Napolitano S, Pilleri A, Rolla P, Wübbenhorst M (2010) ACS Nano 4:841–848
85. Tress M, Erber M, Mapesa EU, Huth H, Müller J, Serghei A, Schick C, Eichhorn K-J, Voit B, Kremer F (2010) Macromolecules 43:9937–9944
86. Raegen A, Massa M, Forrest JA, Dalnoki-Veress K (2008) Eur Phys J E 27:375–377
87. Reiter G, Napolitano S (2010) J Polym Sci B Polym Phys 48:2544
88. McKenna GB (2010) Eur Phys J ST 189:285–302
89. Kim S, Mundra MK, Roth CB, Torkelson JM (2010) Macromolecules 43:5158–5161
90. Rowland H, King W, Pethica J, Cross G (2008) Science 322:720–724
91. Roth CB (2010) J Polym Sci B Polym Phys 48:2558–2560
92. Yang Z, Fujii Y, Lee FK, Lam C-H, Tsui OKC (2010) Science 328:1676–1679
93. Rotella C, Napolitano S, De Cremer L, Koeckelberghs G, Wübbenhorst M (2010) Macromolecules 43:8686–8691
94. Napolitano S, Wübbenhorst M (2011) Nat Commun 2:260
95. Paeng K, Swallen SF, Ediger MD (2011) J Am Chem Soc 133:8444–8447
96. Paeng K, Richert R, Ediger MD (2012) Soft Matter 8:819
97. Siretanu I, Chapel JP, Drummond C (2012) Macromolecules 45:1001–1005
98. Bornside D, Macosko C, Scriven L (1987) J Imaging Technol 13:122–128
99. Croll SG (1979) J Appl Polym Sci 23:847–858
100. Sauer BB, Walsh DJ (1994) Macromolecules 27:432–440
101. de Gennes PG (2002) Eur Phys J E 7:31–34
102. Karim A, Mansour A, Felcher GP, Russell TP (1990) Phys Rev B 42:6846
103. Stamm M, Hüttenbach S, Reiter G, Springer T (1991) Europhys Lett 14:451
104. Reiter G, Steiner U (1991) J Phys II (France) 1:659
105. Russell TP, Deline VR, Dozier WD, Felcher GP, Agrawal G, Wool RP, Mays JW (1993) Nature 365:235
106. de Gennes PG (1992) In: Sanchez IC (ed) Physics of polymer surfaces and interfaces. Butterworth-Heinemann, Boston, p 55
107. Reiter G (1992) Phys Rev Lett 68:75–78; (1993) Langmuir 9:1344–1351
108. de Gennes PG, Brochard-Wyart F, Quéré D (2004) Capillarity and wetting phenomena: drops, bubbles, pearls, waves. Springer, Heidelberg
109. Brochard-Wyart F, di Meglio JM, Quéré D, de Gennes PG (1991) Langmuir 7:335
110. Redon C, Brochard-Wyart F, Rondelez F (1991) Phys Rev Lett 66:715
111. Brochard-Wyart F, Redon C (1992) Langmuir 8:2324
112. Brochard-Wyart F, Martin P, Redon C (1993) Langmuir 9:3682
113. Brochard-Wyart F, de Gennes PG, Hervert H, Redon C (1994) Langmuir 10:1566
114. Lambooy P, Phelan KC, Haugg O, Krausch G (1996) Phys Rev Lett 76:1110
115. Krausch G (1997) J Phys Condens Matter 9:7741
116. Stange TG, Evans DF, Hendrickson WA (1997) Langmuir 13:4459
117. Pan Q, Winey KI, Hu HH, Composto RJ (1997) Langmuir 13:1758
118. Jacobs K, Herminghaus S, Mecke KR (1998) Langmuir 14:965
119. Limary R, Green PF (1999) Langmuir 15:5617
120. Seemann R, Herminghaus S, Jacobs K (2001) Phys Rev Lett 87:196101
121. Vrij A (1966) Discuss Faraday Soc 42:23
122. Brochard-Wyart F, Daillant J (1990) Can J Phys 68:1084
123. Sharma A (1993) Langmuir 9:861; 9:3580
124. Reiter G, Sharma A, Casoli A, David MO, Khanna R, Auroy P (1999) Langmuir 15:2551
125. Reiter G, Sharma A, Casoli A, David MO, Khanna R, Auroy P (1999) Europhys Lett 46:512
126. Reiter G, Khanna R, Sharma A (2000) Phys Rev Lett 85:1432
127. Xie R et al (1998) Phys Rev Lett 81:1251

128. Thiele U, Mertig M, Pompe W (1998) Phys Rev Lett 80:2869
129. Reiter G (1998) Science 282:888
130. Herminghaus S (1999) Phys Rev Lett 83:2359
131. Seemann R, Herminghaus S, Neto C, Schlagowski S, Podzimek D, Konrad R, Mantz H, Jacobs K (2005) J Phys Condens Matter 17:S267
132. De Gennes PG (1985) Rev Mod Phys 57:827
133. Young T (1805) Philos Trans R Soc Lond 95:65
134. Bonn D, Eggers J, Indekeu J, Meunier J, Rolley E (2009) Rev Mod Phys 81:739
135. Huh C, Scriven LE (1971) J Coll Interf Sci 35:85
136. Tanner LH (1979) J Phys D 2:1473
137. de Gennes PG (1979) CR Acad Sci 288B:219
138. Leger L, Joanny JF (1992) Rep Prog Phys 55:431
139. Redon C, Brzoka JB, Brochard-Wyart F (1994) Macromolecules 27:468
140. Raphaël E, de Gennes PG (1992) J Phys Chem 96:4002
141. Brown HR (1994) Science 263:1411
142. Shanahan MER, Carré A (1995) Langmuir 11:1396
143. Debrégeas G, Martin P, Brochard-Wyart F (1995) Phys Rev Lett 75:3886
144. Brochard-Wyart F, Debrégeas G, Fondecave R, Martin P (1997) Macromolecules 30:1211
145. Debrégeas G, de Gennes PG, Brochard-Wyart F (1998) Science 279:1704
146. Reiter G, Khanna R (2000) Langmuir 16:6351
147. Reiter G, Khanna R (2000) Phys Rev Lett 85:2753
148. Casoli A, Brendlé M, Schultz J, Auroy P, Reiter G (2001) Langmuir 17:388
149. Bureau L, Léger L (2004) Langmuir 20:4523
150. Masson J, Green P (2002) Phys Rev Lett 88:205504
151. Rauscher M, Münch A, Wagner B, Blossey R (2005) Eur Phys J E 17:373
152. Fetzer R, Rauscher M, Münch A, Wagner BA, Jacobs K (2006) Europhys Lett 75:638
153. Bäumchen O, Fetzer R, Jacobs K (2009) Reduced interfacial entanglement density affects the boundary conditions of polymer flow. Phys Rev Lett 103:247801
154. Neto C, Evans DR, Bonaccurso E, Butt H-J, Craig VSJ (2005) Rep Prog Phys 68:2859
155. Bäumchen O, Jacobs K (2010) Slip effects in polymer thin films. J Phys Condens Matter 22:033102
156. Leibler L, Ajdari A, Mourran A, Coulon G, Chatenay D (1994) In: Teramoto A, Kobayashi M, Norisuje T (eds) Ordering in macromolecular systems. Springer, Berlin, p 301
157. Shull K (1994) Faraday Discuss 98:203
158. Gay C (1997) Macromolecules 30:5939
159. Ferreira PG, Ajdari A, Leibler L (1998) Macromolecules 31:3994
160. Matsen MW, Gardiner JM (2001) J Chem Phys 115:2794
161. Müller M, MacDowell LG (2001) Europhys Lett 55:221
162. Roth CB, Deh B, Nickel BG, Dutcher JR (2005) Phys Rev E 72:021802
163. Plazek DJ, O'Rourke VM (1971) J Polym Sci Part A2 9:209
164. Bach A, Almdal K, Rasmussen HK, Hassager O (2003) Macromolecules 36:5174
165. Vilmin T, Raphaël E (2006) Phys Rev Lett 97:036105
166. Sun S et al (1980) J Chem Phys 73:5971